

EVOLVING AND INTERACTING DARK ENERGY: PHOTOMETRIC AND SPECTROSCOPIC SYNERGY WITH DES Y3 AND DESI DR2

M. TSEDRIK^{1,2} AND B. BOSE^{1,2}

¹Institute for Astronomy, University of Edinburgh, Royal Observatory, Blackford Hill, Edinburgh, EH9 3HJ, UK and
²Higgs Centre for Theoretical Physics, School of Physics and Astronomy, Edinburgh, EH9 3FD, UK

submitted XXX; accepted YYY

Abstract

We investigate the Dark Scattering (DS) interacting dark energy scenario, characterised by pure momentum exchange between dark matter and dark energy, allowing for a time-dependent equation-of-state described by the Chevallier–Polarski–Linder (CPL) parametrisation. This class of models is weakly constrained by CMB observations and can exhibit distinctive late-time suppression of structure growth. We derive constraints on cosmological, DS, and CPL parameters using three two-point correlation functions from the Dark Energy Survey Year 3 data, combined with baryon acoustic oscillation measurements from DESI, Type Ia supernovae from DES Year 5, and CMB data from Planck. We find the dark-sector interaction parameter A_{ds} to be consistent with zero for all data combinations, and that CPL provides a statistically preferred fit over DS for the selected probes. From the full data combination we obtain $w_0 = -0.76 \pm 0.06$, $w_a = -0.77^{+0.23}_{-0.20}$ for CPL, and $w_0 = -0.79^{+0.05}_{-0.06}$, $w_a = -0.56^{+0.24}_{-0.15}$, ($A_{\text{ds}} = 9.8^{+2.8}_{-9.5}$ bn/GeV) for DS. The inclusion of DES photometric information improves the Figure-of-Merit on (w_0, w_a) by $\sim 20\%$ for CPL and $\sim 50\%$ for DS relative to DESI+SN+CMB alone. We find no evidence for an S_8 discrepancy in either model. These results provide the most stringent pre-Euclid constraints on DS from a combined photometric and spectroscopic analysis.

Keywords: cosmology: theory – cosmology: dark energy – cosmology: observations – large-scale structure of the Universe – methods: statistical

1. INTRODUCTION

The new generation of cosmological surveys such as DESI ¹, Euclid ², and Rubin ³ will deliver Large-Scale Structure (LSS) measurements of unprecedented precision, offering new insights into the nature of the dark sector – dark energy, dark matter and their interactions. The quality of these data will enable decisive tests of the current concordance cosmological model Λ CDM, and will elucidate growing tensions within it (Di Valentino et al. 2025). These tensions include the recent measurement by the DESI experiment that strongly suggests a time-evolving dark energy component (Abdul Karim et al. 2025a) and the recently softened S_8 tension (Wright et al. 2025), a discrepancy between the amplitude of matter fluctuations inferred from LSS observations (Heymans et al. 2021; Abbott et al. 2022a) and the value predicted from Cosmic Microwave Background (CMB) measurements extrapolated to late times within Λ CDM (Planck Collaboration et al. 2020).

Among the proposed extensions to Λ CDM capable of addressing these emerging tensions are interacting dark energy models (Poursidou et al. 2013). These models are also of high theoretical interest as any detection of an interaction would contain valuable information about

the microphysics of the dark sector. In particular, pure momentum exchange, or Type III models, offer distinct phenomenology, allowing for the suppression of structure growth while leaving the background unchanged. This was favorable in light of the S_8 tension, but also provided a more fundamental theoretical model to fit the DESI measurements. A phenomenological representative of these Type III models is the well studied Dark Scattering (DS) model (Simpson 2010), in which dark energy and cold dark matter interact through a pure momentum-exchange mechanism governed by a coupling parameter controlling their cross-section. This coupling modifies the growth of cosmic structure while leaving the background expansion largely unaffected unlike energy-exchange models. The DS framework has been extensively developed through theoretical work, simulations, and data analyses (Baldi & Simpson 2015, 2017; Poursidou & Tram 2016; Kumar & Nunes 2017; Bose et al. 2018; Bose & Taruya 2018; Carrilho et al. 2021; Carrilho et al. 2022; Spurio Mancini & Poursidou 2022; Linton et al. 2022; Tsedrik et al. 2023; Carrilho et al. 2023; Carrion et al. 2024; Tsedrik et al. 2025).

In this study, we investigate an extended DS scenario in which the dark energy equation-of-state evolves with time following the Chevallier–Polarski–Linder (CPL) parametrisation (Chevallier & Polarski 2001; Linder 2003). We constrain this model using the Dark Energy

¹ <https://www.desi.lbl.gov>

² <https://www.euclid-ec.org>

³ <https://rubinobservatory.org>

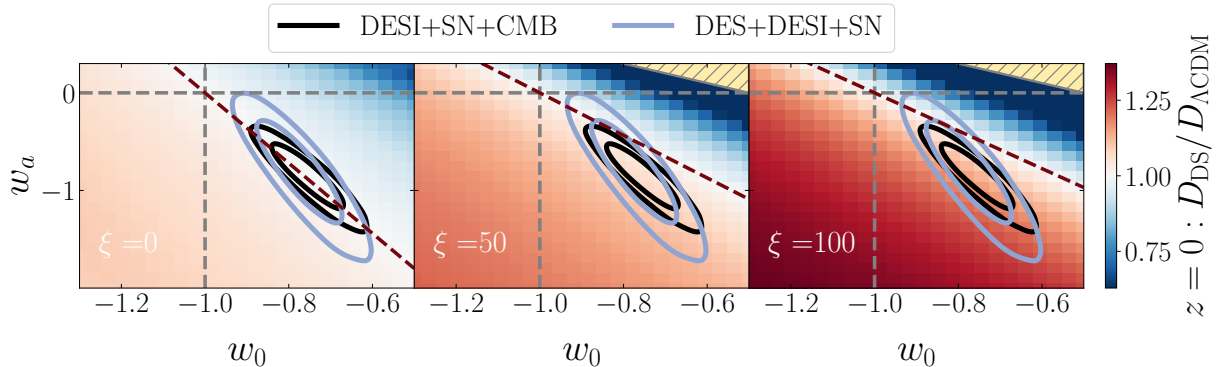


Figure 1. : Linear growth factor in DS with respect to Λ CDM today, overlaid with **official** DESI results for evolving dark energy without interaction (specific combinations of cosmological probes are shown in the legend). The reddish region on the heatmap denotes enhancement of structure growth with respect to Λ CDM, while the blueish region denotes suppression. Grey dashed lines mark the Λ CDM-limit for the dark energy equation-of-state. Dark red dashed line denotes the suppression/enhancement transition, i.e. $D_{\text{DS}} \approx D_{\Lambda\text{CDM}}$, for different values of the interaction strength ξ (in units of [bn/GeV]).

Survey’s ⁴ year 3 (DES Y3) measurements of three two-point correlation functions – cosmic shear, galaxy clustering, and the shear–position cross-correlation – combined with the DR2 DESI BAO data, which has independently shown indications of time-evolving dark energy. This joint analysis leverages the complementarity between photometric and spectroscopic probes to assess both the interaction strength and the evolution of the dark energy component. To model nonlinear structure formation in the DS model with a CPL parametrised equation-of-state, we make use of the halo model reaction formalism (Cataneo et al. 2019) and its associated code ReACT (Bose et al. 2020, [🔗](#)). We construct a neural network emulator using the Cosmopower (Spurio Mancini et al. 2022, [🔗](#)) platform, extending the work of Carrion et al. (2024). We make this emulator public on the ReACT-based emulator repository ([🔗](#)).

This paper is organised as follows: in [section 2](#) we introduce the DS model and its background, linear and nonlinear structure formation predictions; in [section 3](#) we introduce the emulator and describe the data we use; in [section 4](#) we present our results; we conclude and summarize in [section 5](#).

2. MODEL

The Dark Scattering (DS) model is an interacting dark energy scenario in which dark energy and cold dark matter exchange momentum through elastic scattering (Simpson 2010; Pourtsidou et al. 2013; Skordis et al. 2015). Since no energy is transferred between the two components, the background expansion history is not directly altered by the interaction. This form of coupling also has only a mild effect on the CMB, remaining in excellent agreement with Planck measurements (Pourtsidou & Tram 2016).

Compared to Λ CDM, the DS framework introduces two additional parameters: the dark energy equation-of-state w and the interaction strength ξ , the latter defined as the ratio of the scattering cross section to the dark matter particle mass. In this work, we generalise the equation-of-state to evolve in time according to the

CPL parametrisation (Chevallier & Polarski 2001; Linder 2003):

$$w(a) = w_0 + w_a(1 - a), \quad (1)$$

where a is the scale factor and $\{w_0, w_a\}$ are free parameters. This parametrisation allows us to explore scenarios in which dark energy dynamics and momentum exchange jointly affect structure growth. The background expansion in CPL is given by

$$H^2(a) = H_0^2 [\Omega_{\text{m},0} a^{-3} + \Omega_{\text{DE}}], \quad (2)$$

with

$$\Omega_{\text{DE}}(a) = \Omega_{\text{DE},0} e^{\int_1^a 3[1+w(\bar{a})]\bar{a} d\bar{a}}. \quad (3)$$

H_0 is the Hubble constant and $\Omega_{\text{DE},0}$ and $\Omega_{\text{m},0}$ are the present day density parameters of dark energy and total matter respectively, with $\Omega_{\text{DE},0} = 1 - \Omega_{\text{m},0}$ for a flat Universe which we consider in this paper.

The linear perturbations in DS are given by the Continuity and Euler equations (Simpson 2010; Baldi & Simpson 2015; Bose et al. 2018):

$$a\delta' + \theta = 0, \quad (4)$$

$$a\theta' + \left(2 + A + \frac{aH'}{H}\right)\theta - \left(\frac{k}{aH}\right)^2 \Phi = 0, \quad (5)$$

where a prime denotes a scale factor derivative, δ and $\theta = \frac{\nabla \cdot \mathbf{v}}{aH}$ are the linear total density and velocity divergence perturbations, and Φ is the Newtonian gravitational potential. DS introduces an additional term into the Euler equation that controls a frictional force that slows or enhances the evolution of perturbations in LSS depending on the sign of w

$$A(a) \equiv [1 + w(a)] \frac{H_0^2}{H(a)} \frac{3\xi}{8\pi G} \Omega_{\text{DE}}(a), \quad (6)$$

where ξ is a strictly positive parameter that governs the interaction strength in units of [bn/GeV]. The Λ CDM-limit is given by $\xi = 0$ and $w_0 = -1$, $w_a = 0$. In the linearised growth [Equation 5](#) we evolve dark matter and baryons (total matter) as a single species for simplicity. In reality, interaction with dark energy affects dark matter but not baryons in the DS scenario. To take this non-

⁴ <https://www.darkenergysurvey.org/>

universality of coupling into account, we actually suppress the interaction parameter ξ by the dark matter fraction of the total matter, $f_c = \rho_c/\rho_m$ following Carrilho et al. (2022):

$$\bar{\xi} = \frac{f_c}{1 + A(a=1)(1 - f_c)} \xi. \quad (7)$$

We have verified that the linear growth agrees with the modified version of CLASS (♻️) within 1-2% for values of DS parameters within our prior range.

The growth equation can be solved to find the linear growth factor, D , and the growth rate $f \equiv d \ln D / d \ln a$. For the linear growth factor to have a growing solution the frictional force must vanish at high redshifts, i.e. $\lim_{a \rightarrow 0} A(a) \rightarrow 0$. Hence, from Equation 6 we find the condition $w_0 + w_a < -1/2$, which is stronger than the matter-domination condition with $w_0 + w_a < -1$.

In Figure 1 we show for varying values of the interaction parameter the linear growth factor in DS with respect to Λ CDM at $z = 0$. We notice that the suppression/enhancement transition depends on the value of ξ : the suppression of structure growth is observed for approximately $w_a \gtrsim -3.6(1 + w_0)$ with $\xi = 0$, $w_a \gtrsim -2.18(1 + w_0)$ with $\xi = 50$, and $w_a \gtrsim -1.94(1 + w_0)$ with $\xi = 100$. We over-plot official DESI DR2 chains (Abdul Karim et al. 2025b) in the CPL-parametrisation of dark energy without interaction. The tightest constraints are obtained from the joint analysis of BAO with CMB and SN – this combination of (w_0, w_a) values in DS leads to enhancement of structure growth with respect to Λ CDM for all non-zero interaction values (the larger ξ , the stronger the enhancement). Substituting CMB with photometric information from DES Y3, while being less constraining, does not completely exclude the (w_0, w_a) parameter space that yields suppression of structure growth with respect to Λ CDM.

In previous analyses (Carrilho et al. 2023; Carrion et al. 2024; Tsedrik et al. 2025), instead of constraining w_0 and ξ , a new parameter A_{ds} was introduced as

$$A_{\text{ds}} \equiv (1 + w) \xi. \quad (8)$$

This parametrisation allowed for the clearly defined Λ CDM-limit: $A_{\text{ds}} = 0, w_0 = -1$. However, when $w(a)$ is a time-dependent function, A_{ds} also becomes time-dependent. We then must choose a specific value of a at which to define $A_{\text{ds}} \equiv A_{\text{ds}}(a_{\text{ref}})$. In our analyses we will choose the pivot redshift of the main dataset under consideration, in this case DES Y3 + DESI DR2, to define $A_{\text{ds,piv}} \equiv A_{\text{ds}}(a_{\text{piv}})$ with $a_{\text{piv}} \approx 0.72$ ($z_{\text{piv}} \approx 0.4$). This value was computed from the CPL-chain (first column in Table 1) following the same procedure outlined in Abbott et al. (2019). Additionally, we provide constraints on A_{ds} , which in this work denotes $A_{\text{ds}}(a = 1)$.

Moving to nonlinear scales, the scale-independent linear suppression becomes scale dependent (Baldi & Simpson 2015, 2017; Bose et al. 2018; Carrilho et al. 2022). To model these effects, we adopt the halo model reaction formalism (Cataneo et al. 2019). This framework models corrections to the nonlinear power spectrum through a halo model-based reaction function (we refer the reader to Cataneo et al. 2019; Bose et al. 2021; Carrilho et al. 2022, for details). The full nonlinear matter

Table 1: Flat priors for DS-boost emulator. Massive neutrinos are included via the halo model reaction. Baryonic feedback is not included. In the last rows we include additional priors used in the actual analyses.

Parameter	Prior
$\Omega_{\text{m},0}$	[0.22, 0.37]
$\Omega_{\text{b},0}$	[0.03, 0.08]
$\Omega_{\nu,0}$	[0.00015, 0.00317]
h	[0.63, 0.84]
n_s	[0.8, 1.1]
$A_s 10^9$	[1.7, 2.5]
w_0	[-1.3, -0.5]
w_a	[-2, 0.5]
ξ [bn/GeV]	[0, 150]
z	[0, 2.5]
$A_{\text{ds,piv}}$ [bn/GeV]	[-30, 30]
ω_b	$\mathcal{N}(0.02268, 0.00038)$
M_ν [eV]	0.06
τ	$\mathcal{N}(0.054, 0.0074)$

power spectrum is then given by

$$P_{\text{NL}}(k; a) = B(k; a) P_{\text{NL}}^{\Lambda\text{CDM}}(k; a), \quad (9)$$

where the nonlinear boost is given by

$$B(k; a) \equiv \frac{\mathcal{R}(k, a) P^{\text{pseudo}}(k, a)}{P^{\Lambda\text{CDM}}(k, a)}. \quad (10)$$

The reaction function \mathcal{R} , is computed using the halo model reaction code ReACT (Bose et al. 2020, 2023) and includes the effects of massive neutrinos and momentum exchange between dark matter and dark energy. The pseudo power spectrum is a nonlinear Λ CDM spectrum prediction where the initial conditions have been tuned such that the linear clustering at the target redshift matches the beyond- Λ CDM cosmology's linear clustering. Given the scale-independent modification of the linear spectrum in DS, this amounts to changing the amplitude of the input Λ CDM linear spectrum.

The Λ CDM nonlinear ($P^{\Lambda\text{CDM}}$) and pseudo (P^{pseudo}) power spectra are computed in this work using an HMCode2020 (Mead et al. 2021, ♻️) emulator (♻️). The pseudo power spectrum is computed simply by specifying the DS linear power spectrum to HMCode2020. We construct a neural network emulator for $B(k; a)$ to calculate the nonlinear power spectrum efficiently. Details are given in the next section.

3. METHODS AND DATA

3.1. Nonlinear boost emulation

To perform fast cosmological analyses, particularly for weak lensing measurements which require specification of the nonlinear power spectrum, we construct a neural network emulator for Equation 10. This is done using the Cosmopower platform (Spurio Mancini et al. 2022). We keep the same architecture and values of hyperparameters from the original paper.

For the training and validation set boost data, we sample a latin hypercube defined by the parameters and priors given in Table 1. Within this range we generate $1.4 \cdot 10^6$ spectra for the training set, with an additional $6 \cdot 10^4$ generated for testing. We produce boosts in the range $k \in [10^{-2}, 5] h/\text{Mpc}$. We restrict the redshift range and DS parameters based on stability criteria of ReACT. In particular, very low values of σ_8 can result in issues within the spherical collapse part of the code. This has

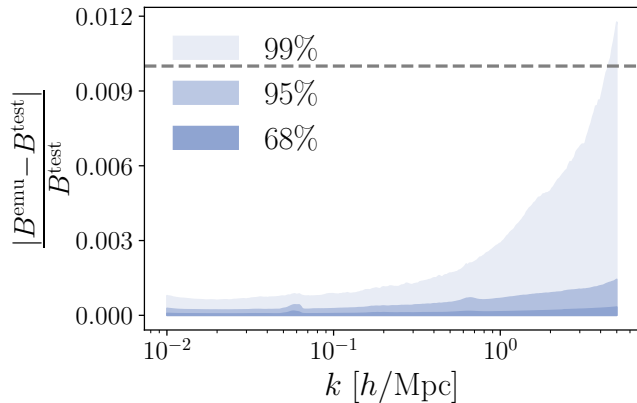


Figure 2. : Quantiles of the relative accuracy of our DS emulator on $6 \cdot 10^4$ testing samples. The dashed grey line denotes the 1% accuracy.

been partly remedied with a [recent patch](#) to the code. The emulator can be found here [🔗](#).

In [Figure 2](#) we show the performance of the emulator on the test data set, indicating that further training data is not needed for our analyses. We note that [Equation 10](#) is at best 1% accurate when compared to simulations at $k \in [0.01, 2] h/\text{Mpc}$ and for $z \in [0, 1]$ for modifications characterised by $\xi \leq 50$ [bn/GeV] ([Carrilho et al. 2022](#)). We have further validated our emulator in the case of $w_a = 0$ against the emulators produced in [Carrión et al. \(2024\)](#) through direct comparison, achieving less than 0.3% agreement for the entire k -range for specific cosmologies. Lastly, a final check was performed by analysing the DES Y3 data for $w_a = 0$ and comparing against the results of [Tsedrik et al. \(2025\)](#), with high agreement of the posteriors obtained. For the latter test, a disagreement in the constraint on A_{ds} (see [Equation 6](#)) was found but this was a function of the prior adopted on ξ . Another difference is that the emulator used in [Tsedrik et al. \(2025\)](#) was trained in A_{ds} and not ξ allowing the exploration of the posterior distribution close to $w \approx -1$ but with $\xi > 150$ bn/GeV. This being said, both results were prior dominated.

3.2. Data sets

In our analyses we consider the following data sets:

DES: We use the publicly available measurements of the three two-point correlation functions ($3 \times 2\text{pt}$) from the third data release of the Dark Energy Survey ([Abbott et al. 2022b, 2023](#)). These include cosmic shear, galaxy clustering, and galaxy-galaxy lensing, measured from sources in four redshift bins and lenses from the first four redshift bins of the MagLim sample ([Porredon et al. 2021](#)). The corresponding covariance matrix is computed analytically following [Friedrich et al. \(2021\)](#), where the methodology is also validated. We adopt the same scale cuts as in the DES Y3 ΛCDM baseline analysis. Our halo model reaction approach to nonlinearities ensures we have sufficient accuracy to probe these scales. We neglect baryonic feedback effects for reasons discussed in [Krause et al. \(2021\)](#).

DESI: We consider all tracers from DESI DR2 BAO ([Abdul Karim et al. 2025b](#)).

CMB: We include *Planck 2018* TT, TE, EE temperature and polarization with *Planck-lite* likelihood

([Prince & Dunkley 2019](#); [Aghanim et al. 2020](#)) including 2 low- ℓ in TT. For cosmological analyses, we apply the Planck-based Gaussian prior on the optical depth of reionization, τ ([Planck Collaboration et al. 2020](#); [Balkenhol 2025](#)). We validate our choice of τ -prior by comparing to a Cobaya chain with full Planck likelihood for DESI+SN+CMB – both in CPL and DS our constraints in τ are not prior dominated. In analyses with CMB we do not impose a BBN prior on ω_b as it is tightly constrained by the CMB information.

SN: We add the full DES Y5 type Ia supernovae sample ([Abbott et al. 2024](#)). This includes 1635 SNe from $z > 0.1$ and 194 SNe at $z < 0.1$.

For our analyses we make use of the official DES pipeline, *CosmoSIS* ([🔗](#)), in which we include two new modules, one which calculates and applies the nonlinear and linear boost factors to the nonlinear and linear power spectra respectively, and one which calculates the linear growth factor and rate. The latter is done using the *MGrowth* ([🔗](#)) code. The boosts are applied to *CAMB* ([Lewis & Challinor 2011](#)) produced linear and *HMCode2020*-based nonlinear spectra. This makes our setup identical to [Tsedrik et al. \(2025\)](#) except we apply a boost rather than emulating the nonlinear and linear spectra directly. CMB observables are computed with the modified version of *CLASS* for DS ([Alessa & Carrilho 2025](#)). For chains without CMB we use *polychord* ([Handley et al. 2015](#)) with “publication quality” settings from [Lemos et al. \(2023\)](#), for chains with CMB we use *Nautilus* ([Lange 2023](#)) with 12000 live points. We changed the sampler due to more efficient convergence of the latter. We cross-checked both samplers in several configurations: contours and $\ln \mathcal{Z}$ were in agreement, while the uncertainty on $\ln \mathcal{Z}$ with *Nautilus* was $\mathcal{O}(10)$ tighter than with *polychord*.

4. RESULTS

We present our full set of results in [Table 1](#) and [Table 2](#) (see Appendix). In all data combinations we find $A_{\text{ds,piv}}$ to be consistent with zero within 1σ . The exception is the DESI+SN+CMB combination, which shows a $\sim 2\sigma$ preference for a non-zero interaction. In this case, the posterior hits the prior boundary because the interaction is unconstrained by background probes and the CMB data set is only very mildly constraining ([Pourtsidou & Tram 2016](#)). This indicates projection effects caused by degeneracies between the standard cosmological and extended parameters ([Gómez-Valent 2022](#); [Hadzhiyska et al. 2023](#); [Carrilho et al. 2023](#)). All combinations also show a preference for (w_0, w_a) in the region favoured by DESI, as expected.

The inclusion of CMB data drives S_8 to slightly higher values, as has been noted previously in the literature (see e.g. [Abbott et al. 2023](#)). Furthermore, the DS model tends to enhance structure growth, pushing S_8 to systematically higher values than in the CPL case. This behaviour is expected given the region of (w_0, w_a) space preferred by DESI data (see [Figure 1](#)). Our CPL results are in good agreement with the DESI results presented in [Abdul Karim et al. \(2025b\)](#) for the DES+DESI+SN and DESI+SN+CMB combinations. The former shows a slight discrepancy in w_a , which we attribute to differences in priors on cosmological parameters between the official DES Y3 analysis ([Abbott et al. 2023](#)) adapted by DESI and our choices summarised in [Table 1](#). An addi-

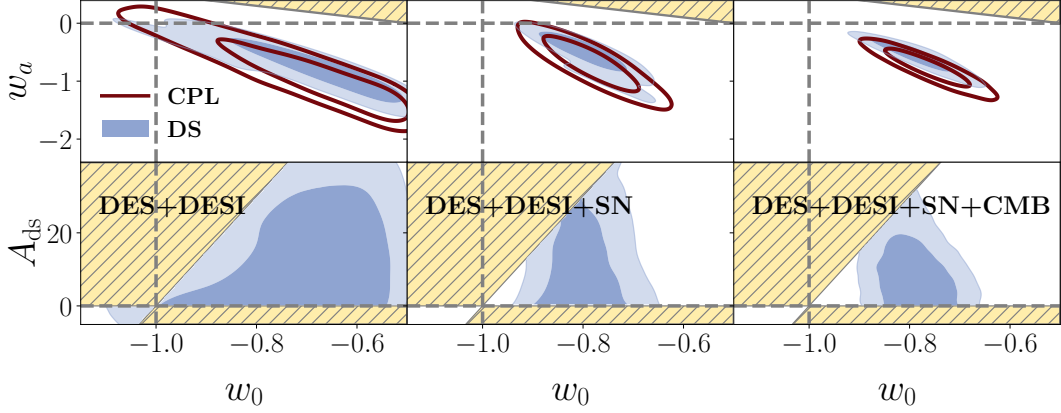


Figure 3. : Dark energy results for different data selections, specified in the legend of the lower panels. CPL constraints are shown in dark red, DS constraints are shown in blue. All contours shown contain 68% and 95% of the posterior probability. Dashed yellow regions denote priors in DS: $w_0 + w_a < -1/2$ for the existence of a growing solution of the linearised growth equation and $0 < \xi < 150$ [bn/GeV].

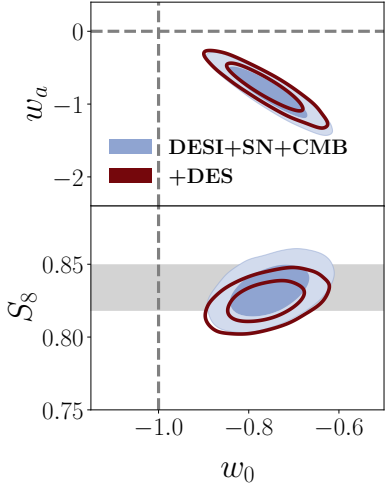


Figure 4. : CPL: constraints without (in blue) and with (in dark red) photometric information from DES. Grey dashed lines denote Λ CDM limit in equation-of-state parameters. Grey stripe denotes constraints from *Planck 2018* without lensing for Λ CDM (Planck Collaboration et al. 2020).

tional, yet less significant, difference between the DESI and our results is the choice of CMB likelihoods.

We further compare DS and CPL in the w_0 - w_a and w_0 - A_{ds} planes in Figure 3. The DS contours are marginally shifted toward higher values of w_a across all combinations with the DES data. Higher values of w_a reduce the enhancement of structure growth induced by the interaction in this region of (w_0, w_a) space (see Figure 1). Since DES data prefers slightly lower values of S_8 , this leads to a mild shift in the DS contours. The extent of the shift is restricted by SN data which prefers lower values of w_a . We note here that recalibration of the DES Y5 SN may weaken its preference for more negative values of w_a (Popovic et al. 2025).

This behaviour is further illustrated in Figure 4 and Figure 5, which show the impact of DES on the w_0 , w_a , and S_8 constraints for CPL and DS, respectively. In the CPL case, we find that DES does not significantly improve constraints on w_0 or w_a (or S_8) consistent with

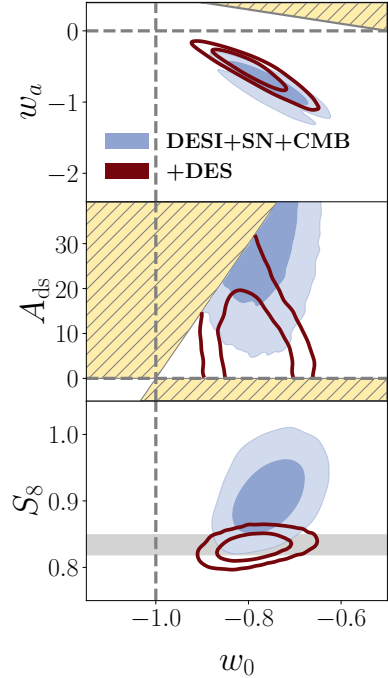


Figure 5. : Same as Figure 4 for DS. Dashed yellow regions denote prior constraints same as in Figure 3.

the findings of Abbott et al. (2023). In DES, the preference for S_8 values mildly lower than the ones extrapolated from DESI+SN+CMB appears to tighten constraints on S_8 in the full combination of probes and lead to a slight improvement in (w_0, w_a) . In contrast, for the DS model, the inclusion of DES removes the $\sim 2\sigma$ preference for non-zero A_{ds} seen in the background+CMB combination, and consequently tightens the S_8 constraint towards lower values. This is also reflected in the improvement of the Figure-of-Merit (FoM) when adding the DES data to the DESI+CMB+SN combination. In CPL we find $\text{FoM}=140.65 \rightarrow \text{FoM}=167.66$ which constitutes a 19.2% improvement by including DES. For DS we have $\text{FoM}=140.43 \rightarrow \text{FoM}=215.39$ which is a much larger 53.4% improvement, highlighting how the model requires structure formation data in order to be constrained. As

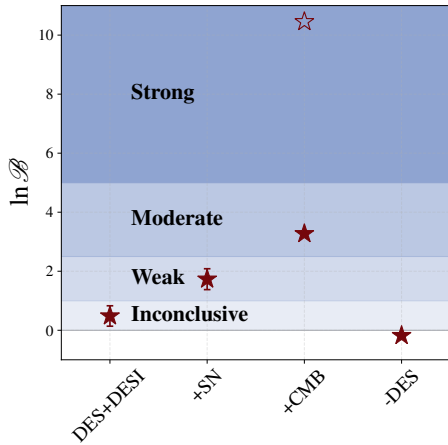


Figure 6. : The Bayes factor: $\ln \mathcal{B} = \ln \mathcal{Z}_{\text{CPL}} - \ln \mathcal{Z}_{\text{DS}}$. Errorbars correspond to 68% c.l. provided by the samplers. The shaded regions denote the Jeffreys' scale thresholds for evidence interpretation, i.e. significance of CPL being better supported by data than DS: $0 < \ln \mathcal{B} < 1$ (inconclusive), $1 < \ln \mathcal{B} < 2.5$ (weak), $2.5 < \ln \mathcal{B} < 5$ (moderate), and $\ln \mathcal{B} > 5$ (strong). The filled stars denote DS with the evolving equation-of-state, while the hollow star denotes DS with the constant equation-of-state.

with previous analyses (see for example [Tsedrik et al. 2025](#)) we find no signs of the S_8 tension nor of interaction.

Finally, in [Figure 6](#) we present the Bayes factor comparing CPL and DS across different data combinations. Shaded regions represent the Jeffreys' scale thresholds for the Bayes factor interpretation ([Trotta 2008](#)). These results show that DS does not alleviate the mild preference for lower S_8 values from DES when CMB data are included, as the interaction enhances structure growth in the region of (w_0, w_a) space favoured by DESI. Adding SN+CMB data to DES+DESI increases the preference for CPL over DS from negligible to moderate, while removing DES reduces this preference back to negligible.

For the full data combination we repeat the analysis in DS with the constant equation-of-state. In agreement with [Abdul Karim et al. \(2025b\)](#), for a w_0 CDM background and this combination of probes we obtain $w_0 \approx -0.96$, Ω_m lower and h higher than in $w_0 w_a$ CDM. In this scenario, for $w_0 > -1$, any non-zero interaction between dark matter and dark energy leads to suppression of LSS growth at late times. Hence, we obtain a low value of S_8 not supported by the data. Overall, CPL shows strong evidence over DS with constant $w(a) = w_0$. The corresponding posterior distributions in all cosmological parameters for the full combination of probes is shown in [Figure 1](#) of Appendix.

5. CONCLUSIONS

In this paper we combine the 3×2 pt correlation functions of DES Y3, and the BAO measurements of DESI DR2, together with DES Y5 SN and Planck CMB, in order to constrain the DS model – a momentum exchange interacting dark energy model. For reference we compare our results for each data combination with constraints from the CPL model. Both DS and CPL have the same background evolution, with the equation-of-state for dark energy given by $w = w_0 + w_a(1 - a)$. DS includes an ad-

ditional parameter, A_{ds} or ξ , which controls the strength of the coupling between dark matter and dark energy. This parameter does not depend on the background observables, SN and BAO, and only weakly modifies low- ℓ and lensing in CMB. However, the non-zero interaction parameter enhances or suppresses growth of structures in a way, which depends on values of the equation-of-state parameters. Hence, cosmological probes, which contain information on the time-evolution of LSS growth, are essential to constrain DS and differentiate it from CPL.

From the full combination of cosmological probes we obtain the following constraints: $w_0 = -0.76 \pm 0.06$ and $w_a = -0.77^{+0.23}_{-0.20}$ for CPL, $w_0 = -0.79^{+0.05}_{-0.06}$, $w_a = -0.56^{+0.24}_{-0.15}$, and $A_{\text{ds}} = 9.8^{+2.8}_{-9.5}$ bn/GeV for DS. There is no detection of interaction, with A_{ds} being consistent with zero. Moreover, the equation-of-state parameter space preferred by DESI+SN+CMB, leads to enhancement of structure growth for non-zero A_{ds} . This dependence between (w_0, w_a) and A_{ds} drifts the constraints in w_a towards less negative values than in CPL in an attempt to cross the enhancement/suppression transition we show in [Figure 1](#). However, the combined signal from DESI+SN favours a restricted region in (w_0, w_a) space. We note that the DES Y5 SN sample we use in our analysis has been recently re-calibrated ([Popovic et al. 2025](#)). This might result in slightly less negative values of w_a and a (w_0, w_a) combination that allows a potential scattering signal. Hence, we treat our constraints from the chosen data combination as rather pessimistic for DS detection and leave the investigation with the re-calibrated sample for future work.

We quantify the role of LSS-growth data, by assessing the FoM in (w_0, w_a) without and with addition of the 3×2 pt information from DES to DESI+SN+CMB. For CPL, the improvement in constraints with DES is not significant: $\sim 20\%$. This is similar to the addition of the full-shape information from the spectroscopic measurements of galaxy distributions ([Chudaykin et al. 2025](#)). However, for DS this number increases up to $\sim 50\%$ due to the constraining power in A_{ds} through the well-measured amplitude, S_8 .

Both in CPL and DS, we find no evidence for the S_8 tension. This is consistent with our previous findings in [Tsedrik et al. \(2025\)](#). The constraints on this late-time amplitude agree well with the predictions from CMB in Λ CDM. For CPL, the (w_0, w_a) values remain on the already established region that DESI+SN+CMB prefer, which falls on a line in (w_0, w_a) space that gives no relative change to growth over Λ CDM. For DS, this growth-enhancement/suppression line is a function of the scattering amplitude, with the preferred region of (w_0, w_a) values lying in the enhancement regime. Consequently, DS would be preferred if the DES measurement of S_8 would be higher than the one derived from the CMB constraints. This is the opposite of the observed trend in other lensing data sets (e.g. Hyper Suprime-Cam [Dalal et al. 2023](#); Sugiyama et al. 2023; Miyatake et al. 2023; Li et al. 2023).

While providing consistent constraints on shared cosmological parameters, the preference for CPL over DS becomes clear by evaluation of the Bayes factor. In all data combinations with DES, CPL is preferred by data, consistent with the argumentation in the previous para-

graph. Additionally, we perform an analysis for the constant equation-of-state in DS with the full combination of probes – CPL remains better supported by the data in this case too.

There are alternative interacting dark energy models, such as the one discussed in [Li & Zhang \(2025\)](#). There, dark energy and dark matter exchange both momentum and energy, while the equation-of-state for dark energy is fixed to $w = -1$. The flow of energy between dark matter and dark energy reverses direction in the late-time Universe. The authors claim that this model explains DESI+SN+CMB measurements as well as CPL. However, the parameter space in the “sign-reversal” model preferred by this combination of data ultimately leads to low values of S_8 – hence less preferable by DES 3×2 pt baseline analysis. This highlights an importance of structure growth information in constraining interacting dark energy models. With the new generation of photometric surveys like Euclid and Rubin, we will have more certainty in whether and how dark energy and dark matter interact.

ACKNOWLEDGEMENTS

The authors are grateful to the DESI and DES collaborations for making their data publicly available. The authors thank Pedro Carrilho for valuable comments, and Durrah Alessa for a discussion on the PPF framework with interacting dark energy. BB is supported by a UK Research and Innovation Stephen Hawking Fellowship (EP/W005654/2). MT’s research is supported by grant ST/Y000986/1. For the purpose of open access, the author has applied a Creative Commons Attribution (CC BY) license to any Author Accepted Manuscript version arising from this submission.

DATA AVAILABILITY

Links and references with sources of the data and analysis pipelines are provided in the main text.

REFERENCES

- Abbott T. M. C., et al., 2019, *Phys. Rev. D*, 99, 123505
 Abbott T. M. C., et al., 2022a, *Phys. Rev. D*, 105, 023520
 Abbott T. M. C., et al., 2022b, *Phys. Rev. D*, 105, 023520
 Abbott T. M. C., et al., 2023, *Phys. Rev. D*, 107, 083504
 Abbott T. M. C., et al., 2024, *Astrophys. J. Lett.*, 973, L14
 Abdul Karim M., et al., 2025a, DESI DR2 Results II: Measurements of Baryon Acoustic Oscillations and Cosmological Constraints ([arXiv:2503.14738](#))
 Abdul Karim M., et al., 2025b, *Phys. Rev. D*, 112, 083515
 Aghanim N., et al., 2020, *Astron. Astrophys.*, 641, A5
 Alessa D., Carrilho P., 2025, *Edinburgh Student Journal of Science*, 1, 7
 Baldi M., Simpson F., 2015, *MNRAS*, 449, 2239
 Baldi M., Simpson F., 2017, *MNRAS*, 465, 653
 Balkenhol L., 2025, *The Open Journal of Astrophysics*, 8, 17
 Bose B., Taruya A., 2018, *J. Cosmology Astropart. Phys.*, 10, 019
 Bose B., Baldi M., Pourtsidou A., 2018, *J. Cosmology Astropart. Phys.*, 2018, 032
 Bose B., Cataneo M., Tröster T., Xia Q., Heymans C., Lombriser L., 2020, *MNRAS*, 498, 4650
 Bose B., et al., 2021, *MNRAS*, 508, 2479
 Bose B., Tsedrik M., Kennedy J., Lombriser L., Pourtsidou A., Taylor A., 2023, *Mon. Not. Roy. Astron. Soc.*, 519, 4780
 Carrilho P., Moretti C., Bose B., Marković K., Pourtsidou A., 2021, *J. Cosmology Astropart. Phys.*, 2021, 004
 Carrilho P., Carrion K., Bose B., Pourtsidou A., Hidalgo J. C., Lombriser L., Baldi M., 2022, *MNRAS*, 512, 3691
 Carrilho P., Moretti C., Pourtsidou A., 2023, *J. Cosmology Astropart. Phys.*, 2023, 028
 Carrion K., Carrilho P., Spurio Mancini A., Pourtsidou A., Hidalgo J. C., 2024, *MNRAS*, 532, 3914
 Cataneo M., Lombriser L., Heymans C., Mead A., Barreira A., Bose S., Li B., 2019, *MNRAS*, 488, 2121
 Chevallier M., Polarski D., 2001, *Int. J. Mod. Phys. D*, 10, 213
 Chudaykin A., Ivanov M. M., Philcox O. H. E., 2025, arXiv e-prints
 Dalal R., et al., 2023, *Phys. Rev. D*, 108, 123519
 Di Valentino E., et al., 2025, The CosmoVerse White Paper: Addressing observational tensions in cosmology with systematics and fundamental physics ([arXiv:2504.01669](#)), [doi:10.1016/j.dark.2025.101965](#)
 Friedrich O., et al., 2021, *MNRAS*, 508, 3125
 Gómez-Valent A., 2022, *Phys. Rev. D*, 106, 063506
 Hadzhiyska B., Wolz K., Azzoni S., Alonso D., García-García C., Ruiz-Zapatero J., Slosar A., 2023, *The Open Journal of Astrophysics*, 6, 23
 Handley W. J., Hobson M. P., Lasenby A. N., 2015, *MNRAS*, 450, L61
 Heymans C., et al., 2021, *A&A*, 646, A140
 Krause E., et al., 2021, arXiv e-prints, p. arXiv:2105.13548
 Kumar S., Nunes R. C., 2017, *Eur. Phys. J. C*, 77, 734
 Lange J. U., 2023, *MNRAS*, 525, 3181
 Lemos P., et al., 2023, *MNRAS*, 521, 1184
 Lewis A., 2025, *JCAP*, 08, 025
 Lewis A., Challinor A., 2011, *CAMB*, ascl:1102.026
 Li Y.-H., Zhang X., 2025, *JCAP*, 12, 018
 Li X., et al., 2023, *Phys. Rev. D*, 108, 123518
 Linder E. V., 2003, *Phys. Rev. Lett.*, 90, 091301
 Linton M. S., Crittenden R., Pourtsidou A., 2022, *J. Cosmology Astropart. Phys.*, 08, 075
 Mead A., Brieden S., Tröster T., Heymans C., 2021, *MNRAS*, 502, 1401
 Miyatake H., et al., 2023, *Phys. Rev. D*, 108, 123517
 Planck Collaboration et al., 2020, *A&A*, 641, A6
 Popovic B., et al., 2025, arXiv e-prints
 Porredon A., et al., 2021, *Phys. Rev. D*, 103, 043503
 Pourtsidou A., Tram T., 2016, *Phys. Rev. D*, 94, 043518
 Pourtsidou A., Skordis C., Copeland E. J., 2013, *Phys. Rev. D*, 88, 083505
 Prince H., Dunkley J., 2019, *Phys. Rev. D*, 100, 083502
 Simpson F., 2010, *Phys. Rev. D*, 82, 083505
 Skordis C., Pourtsidou A., Copeland E. J., 2015, *Phys. Rev. D*, 91, 083537
 Spurio Mancini A., Pourtsidou A., 2022, *MNRAS*, 512, L44
 Spurio Mancini A., Piras D., Alsing J., Joachimi B., Hobson M. P., 2022, *MNRAS*, 511, 1771
 Sugiyama S., et al., 2023, *Phys. Rev. D*, 108, 123521
 Trotta R., 2008, *Contemp. Phys.*, 49, 71
 Tsedrik M., Moretti C., Carrilho P., Rizzo F., Pourtsidou A., 2023, *MNRAS*, 520, 2611
 Tsedrik M., et al., 2025, *MNRAS*
 Wright A. H., et al., 2025, KiDS-Legacy: Cosmological constraints from cosmic shear with the complete Kilo-Degree Survey ([arXiv:2503.19441](#))

APPENDIX

This paper was built using the Open Journal of Astrophysics L^AT_EX template. The OJA is a journal which provides fast and easy peer review for new papers in the astro-ph section of the arXiv, making the reviewing process simpler for authors and referees alike. Learn more at <http://astro.theoj.org>.

Table 1: Mean values and 68% c.l. values for CPL and DS with fixed one massive neutrino with $M_\nu = 0.06$ eV for the different combination of probes considered in this work. The values are computed with `getdist` (Lewis 2025, ) with imposed ranges from Table 1. We show the maximum *a posteriori* values from the chains in parentheses. In the second vertical block, we include derived constraints on A_{ds} (Equation 8 at $z = 0$), σ_8 , $S_8 = \sigma_8 \sqrt{\Omega_m/0.3}$, $\ln(10^{10} A_s)$. We report the number of data-points N_{data} , the number of parameters N_{par} varied in the MCMC, and log-evidence $\ln \mathcal{Z}$ from the sampler. Unconstrained parameters are denoted by a dash-line. The BBN prior is applied, sampled with `polychord`.

N_{data}	DES+DESI 462+13		DES+DESI+SN 462+13+1829	
	CPL	DS	CPL	DS
Ω_m	$0.330^{+0.019}_{-0.012}(0.337)$	$0.327^{+0.016}_{-0.012}(0.357)$	$0.321 \pm 0.009(0.313)$	$0.317 \pm 0.008(0.323)$
$\omega_b \cdot 10^2$	$2.27 \pm 0.04(2.23)$	$2.27 \pm 0.04(2.26)$	$2.27 \pm 0.04(2.27)$	$2.27 \pm 0.04(2.26)$
w_0	$> -0.740(-0.643)$	$-0.688^{+0.18}_{-0.048}(-0.5)$	$-0.782 \pm 0.063(-0.795)$	$-0.792^{+0.051}_{-0.059}(-0.764)$
w_a	$-0.93^{+0.33}_{-0.58}(-1.37)$	$-0.78^{+0.32}_{-0.41}(-1.4)$	$-0.71^{+0.33}_{-0.29}(-0.66)$	$-0.54^{+0.30}_{-0.18}(-0.78)$
$A_{\text{ds,piv}}$	0	$5.4^{+2.5}_{-5.8}(0.9)$	0	$4.0^{+1.9}_{-4.7}(0.5)$
$A_s \cdot 10^9$	-(1.741)	-(1.804)	-(1.993)	-(1.804)
h	$0.664^{+0.012}_{-0.017}(0.673)$	$0.655^{+0.009}_{-0.017}(0.672)$	$0.674 \pm 0.009(0.664)$	$0.667 \pm 0.009(0.676)$
n_s	$0.962^{+0.039}_{-0.045}(0.951)$	$0.988 \pm 0.040(0.942)$	$0.962 \pm 0.043(1.004)$	$0.989^{+0.043}_{-0.038}(0.946)$
A_{ds}	0	$17.0^{+6.7}_{-17}(4.4)$	0	$12.2^{+4.5}_{-12}(7.9)$
σ_8	$0.777^{+0.018}_{-0.026}(0.773)$	$0.781^{+0.019}_{-0.022}(0.740)$	$0.785^{+0.016}_{-0.021}(0.791)$	$0.790 \pm 0.018(0.788)$
S_8	$0.814 \pm 0.015(0.819)$	$0.816 \pm 0.018(0.808)$	$0.811 \pm 0.015(0.808)$	$0.812 \pm 0.017(0.818)$
$\ln(10^{10} A_s)$	-(2.857)	-(2.893)	-(2.992)	-(2.893)
N_{par}	29	30	29	30
$\ln \mathcal{Z}$	5740.1 ± 0.2	5739.6 ± 0.2	4915.3 ± 0.2	4913.5 ± 0.2

Table 2: Same as above but for data combinations with CMB. The BBN prior is not applied, sampled with `Nautilus`. Additionally considered is DS with constant equation-of-state, i.e. $w_a = 0$ and $A_{\text{ds,piv}} = A_{\text{ds}}$.

N_{data}	DESI+SN+CMB 13+1829+615		DES+DESI+SN+CMB 462+13+1829+615		
	CPL	DS	CPL	DS	DS
Ω_m	$0.319 \pm 0.006(0.323)$	$0.319 \pm 0.006(0.318)$	$0.318 \pm 0.005(0.316)$	$0.318 \pm 0.005(0.321)$	$0.310 \pm 0.005(0.312)$
$\omega_b \cdot 10^2$	$2.24 \pm 0.01(2.22)$	$2.25 \pm 0.01(2.28)$	$2.24 \pm 0.01(2.26)$	$2.25 \pm 0.01(2.24)$	$2.25 \pm 0.01(2.24)$
w_0	$-0.753 \pm 0.058(-0.758)$	$-0.754 \pm 0.052(-0.694)$	$-0.762 \pm 0.056(-0.821)$	$-0.789^{+0.048}_{-0.056}(-0.735)$	$-0.959^{+0.018}_{-0.026}(-0.953)$
w_a	$-0.84^{+0.25}_{-0.22}(-0.85)$	$-0.76^{+0.22}_{-0.16}(-0.93)$	$-0.77^{+0.23}_{-0.20}(-0.51)$	$-0.56^{+0.24}_{-0.15}(-0.71)$	0
$A_{\text{ds,piv}}$	0	-(6.3)	0	$3.0^{+1.0}_{-3.1}(1.2)$	$1.1^{+0.3}_{-1.1}(1.2)$
$A_s \cdot 10^9$	$2.109 \pm 0.029(2.081)$	$2.099 \pm 0.030(2.087)$	$2.098 \pm 0.027(2.081)$	$2.090 \pm 0.028(2.057)$	$2.112 \pm 0.028(2.121)$
h	$0.668 \pm 0.006(0.666)$	$0.666^{+0.005}_{-0.006}(0.666)$	$0.668 \pm 0.006(0.669)$	$0.666 \pm 0.005(0.661)$	$0.673 \pm 0.005(0.670)$
n_s	$0.966 \pm 0.004(0.967)$	$0.968 \pm 0.004(0.969)$	$0.968 \pm 0.004(0.968)$	$0.970 \pm 0.004(0.972)$	$0.972 \pm 0.003(0.975)$
A_{ds}	0	-(44.8)	0	$9.8^{+2.8}_{-9.5}(4.9)$	$1.1^{+0.5}_{-1.1}(1.2)$
σ_8	$0.807 \pm 0.010(0.808)$	$0.881^{+0.032}_{-0.040}(0.925)$	$0.801 \pm 0.009(0.791)$	$0.808^{+0.013}_{-0.014}(0.790)$	$0.785 \pm 0.011(0.784)$
S_8	$0.832 \pm 0.012(0.839)$	$0.909^{+0.034}_{-0.041}(0.953)$	$0.825 \pm 0.009(0.812)$	$0.831 \pm 0.014(0.818)$	$0.797^{+0.010}_{-0.009}(0.799)$
$\ln(10^{10} A_s)$	$3.049 \pm 0.014(3.035)$	$3.044 \pm 0.014(3.038)$	$3.044 \pm 0.013(3.035)$	$3.040 \pm 0.013(3.024)$	$3.050 \pm 0.013(3.054)$
N_{par}	8	9	30	31	30
$\ln \mathcal{Z}$	-1140.659 ± 0.006	-1140.480 ± 0.006	4612.566 ± 0.006	4609.294 ± 0.006	4602.111 ± 0.006

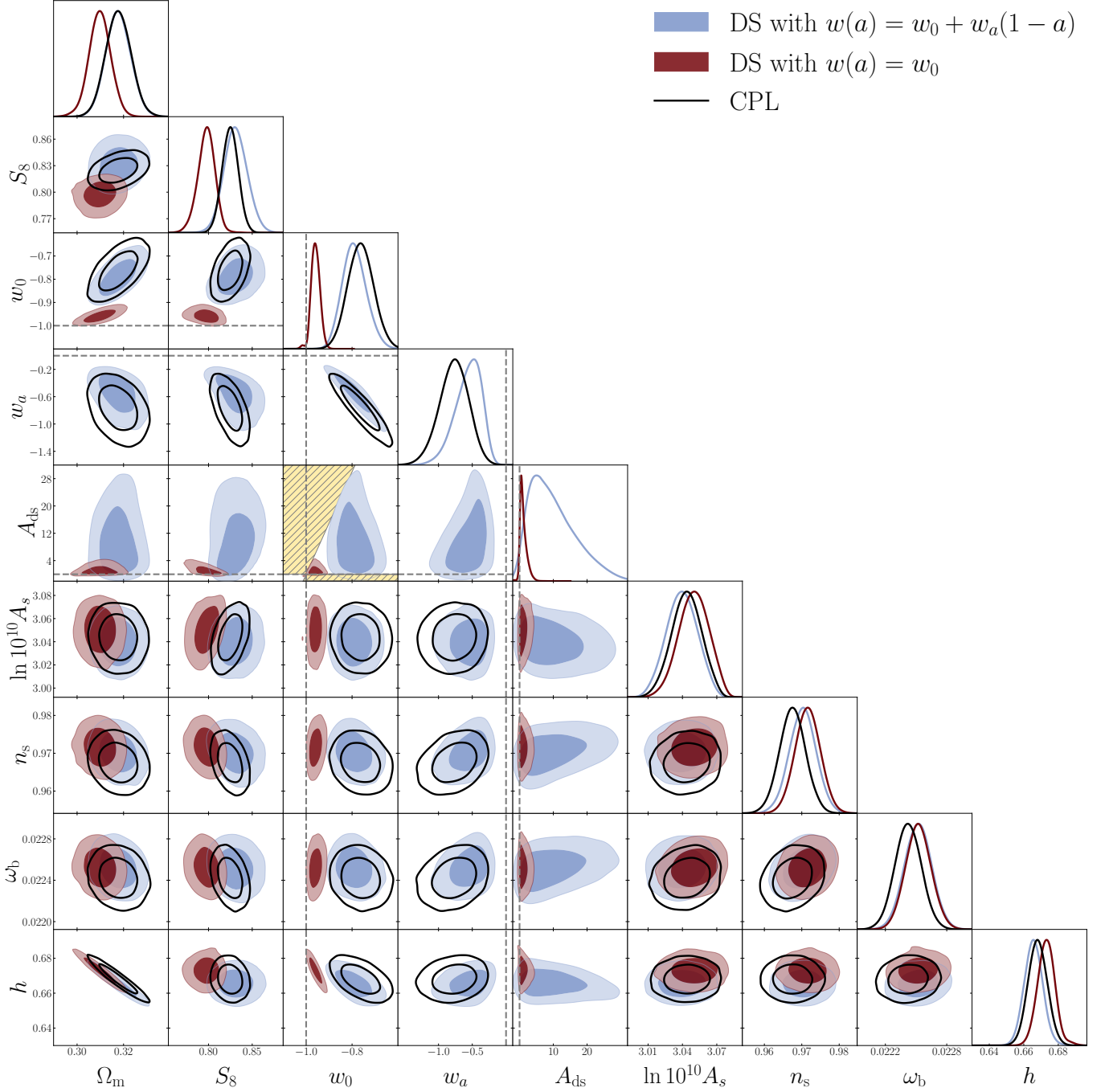


Figure 1. : Dark energy results with the full combination of cosmological probes – DES+DESI+SN+CMB – for different models, specified in the legend. CPL constraints are shown in black, DS constraints with $(w_0 w_a)$ are shown in blue and DS with the constant equation-of-state in dark red. All contours shown contain 68% and 95% of the posterior probability. Dashed yellow regions denote priors in DS: $w_0 + w_a < -1/2$ for the existence of a growing solution of the linearised growth equation and $0 < \xi < 150$ [bn/GeV]. Dashed grey lines denote the Λ CDM limit in $(w_0 w_a)$ and A_{ds} .